

## RESISTIVE-WALL IMPEDANCE OF INSERTIONS FOR FCC-HH\*

B. Riemann<sup>†</sup>, S. Khan, DELTA, Dortmund, Germany  
 S. Arsenyev, D. Schulte, CERN, Geneva, Switzerland

### Abstract

In this work, transverse and longitudinal resistive-wall impedances for beam pipes in the experiment, injection, extraction and RF systems insertion regions of the Future Hadron-Hadron Collider (FCC-hh, see Fig. 1) are computed based on contributions from different given cross sections of the surrounding (elliptical) chamber parts along the beam path, their temperature-dependent conductivities, and optical functions. An emphasis is placed on the behaviour of transverse impedance in the main experimental regions (A and G), where maximum beta values of  $10^4$  m to  $10^5$  m occur in dependence of the operation mode respectively lattice configuration. Main contributions to the transverse and longitudinal impedance budget are identified, and possibilities of reducing them are discussed.

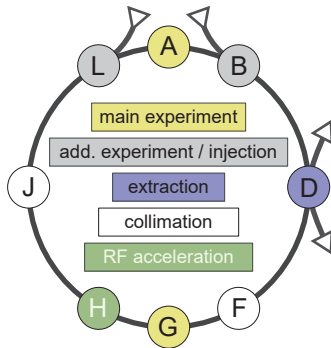


Figure 1: Insertion topology of the Future Hadron-Hadron Collider (FCC-hh) based on [1]

### THEORY

The standard treatment of wakefields in a chamber with varying cross-section and infinitely thick walls with finite resistivity  $\rho$  is pursued, neglecting both resonance behaviour of chamber parts above cutoff frequencies of the chamber waveguide and also effects of skin depth for chamber walls with finite thickness as described in [2].

#### Transverse Wall Impedance

The transverse wall impedance per unit length in a circular tube of radius  $b$  can be approximated<sup>1</sup> by [3, 4]

$$\frac{Z_{\perp}^{\circ}(f)}{L} = Z_0 \delta_{\text{skin}} \frac{1 + i \operatorname{sign} f}{2\pi b^3}$$

\* Work supported by German Ministry of Education & Research (BMBF, funding code 05P15PERB1) and CERN (reference numbers KE3123, EDMS 1606722).

<sup>†</sup> bernard.riemann@tu-dortmund.de

<sup>1</sup> Note that the sign of the imaginary part depends on the definition of the field time-dependence  $\exp(i\omega t)$ . In [3], the sign differs due to the time-dependence  $\exp(-i\omega t)$ .

with skin depth  $\delta_{\text{skin}}(f) \propto \sqrt{\rho/f}$  and the electrical resistivity of the material  $\rho$ . The frequency scaling law is limited by inductive bypass (low frequencies) [2] and resonant structures (high frequencies); for the cold beamscreen [5], the valid frequency range for this scaling law includes [ $10^4$  Hz,  $10^7$  Hz].

For elliptical cross-sections of a beam tube with semiaxes  $w, b$ , approximate values are obtained by multiplication of circular-pipe impedances with form factors  $G_{1x}(q), G_{1y}(q)$  as defined in [6] (see also [7])

$$\frac{Z_{\perp}(f)}{L} = G_{1\perp}(q) Z_{\perp}^{\circ}(f) \quad \text{with } q = \frac{w-b}{w+b}.$$

This expression is inserted into the single-kick model for transverse impedances originating from [4]

$$Z_{\perp} = \frac{1}{\beta_{\perp}^{\text{smooth}}} \sum_j \beta_{\perp}(s_j) Z_{\perp,j}.$$

To compute a better approximation of an element's contribution to impedance, a transition to the continuum along  $s$  is performed, keeping resistivities and chamber geometries as step-wise constant quantities, but approximating  $\beta(s)$  as a 3<sup>rd</sup> order polynomial. As optics codes routinely compute optical functions between elements, the integral is resolved using the approach of Gaussian quadrature as

$$\int_0^L \beta(s) ds \approx L \frac{\beta(L) + \beta(0)}{2} + L^2 \frac{\alpha(L) - \alpha(0)}{6}.$$

Note that this approximation is exact for drift spaces, inside which  $\beta(s)$  is just a quadratic polynomial.

With the aforementioned approximations and the additional assumption  $\mu_r \approx 1$ , the total transverse wall impedance reduces to

$$Z_{\perp}(f) = \zeta_{\perp} \frac{1 + i \operatorname{sign}(f)}{\sqrt{f}}$$

$$\text{with } \zeta_{\perp} = \frac{Z_0}{2\pi^{3/2} \sqrt{\mu_0} \beta_{\perp}^{\text{smooth}}} \sum_j \left( \frac{G_{1\perp} \sqrt{\rho}}{b^3} \int \beta(s) ds \right)_j.$$

$\zeta_{\perp}$  is a constant that fully characterizes the frequency dependence for given geometry and material.

#### Longitudinal Wall Impedance

With the aforementioned approximations, the longitudinal impedance for a circular chamber is given as [3, 8]

$$\frac{Z_{\parallel}(\omega)}{L} = \frac{1}{2b} \frac{Z_0}{\pi c} \sqrt{\frac{\pi \rho f}{\mu_0}} (1 + i \operatorname{sign} f).$$

For a chamber with elliptical cross section, the impedance is multiplied with the respective longitudinal form factor  $G_0(q)$  [6]. This yields ( $f \geq 0$ )

$$Z_{\parallel}(f) = \alpha(1+i)\sqrt{f}, \text{ with} \quad (1)$$

$$\alpha = \frac{Z_0}{2\pi c} \sqrt{\frac{\pi}{\mu_0}} \sum_j \left( \frac{G_0\sqrt{\rho}}{b} \right) (s_j - s_{j-1})$$

where, again, piecewise constant apertures and resistivities for  $s \in ]s_{j-1}, s_j]$  have been assumed.

## COMPUTATION FOR FCC-HH

Using the information supplied in [5], a circumference  $U = 97.749$  km and full betatron tunes  $Q_{\perp} = (111.3, 109.3)$  are assumed to determine  $\beta_{\perp}^{smooth} = U/(2\pi Q_{\perp})$  for the following considerations. The wall material is assumed to possess the resistivity of copper at two different temperatures [9]

$$\rho(T = 50 \text{ K}) = 0.518 \text{ n}\Omega \text{ m},$$

$$\rho(T = 293 \text{ K}) = 16.78 \text{ n}\Omega \text{ m}.$$

Drift spaces are always assumed as having a chamber temperature of 293 K, while the treatment of magnets<sup>2</sup> depends on the considered insertion (A,G,B,L: 50 K, D: 293 K). All other lattice elements are ignored.

After input for previous manual iterations [10], the assumed optical function values and cross sections are directly obtained from the FCC-hh lattice [11] with additional aperture input for region A [12].<sup>3</sup>

In the provided input files, the chamber cross sections are defined by an ellipse, a rectangle, or by intersection of an ellipse and a rectangle. All these cross-section types are approximated as elliptical, taking the minimal extension of the cross section in cartesian directions as semi-axes. Numerically integrated form factors were truncated after the first 50 summands. For elements with missing aperture information, the cross section is assumed as circular with  $b = 40$  mm radius.

### Integrated Results by Operation Modes

The optics in [11] are classified by the  $\beta$  value in the collision point of experiment A, called  $\beta^*$ . The integrated transverse impedance coefficients of all insertions are shown in Tab. 1. The integrated longitudinal coefficient is

$$12.035 \text{ } \Omega/\sqrt{\text{MHz}}.$$

As can be observed in the aforementioned table, lower  $\beta^*$  generally causes higher transverse impedance for the collider optics due to stronger focusing (see sec. ).

The collision mode with  $\beta^* = 0.3$  m and the injection mode with  $\beta^* = 4.6$  m are investigated in more detail in the following. Their impedance coefficients are compared to effective coefficients for the cold beamscreen impedance [5] for collision optics (Tab. 2) and for injection optics (Tab. 3).

<sup>2</sup> lattice elements QUADRUPOLE, RBEND, SBEND, HKICKER, VKICKER  
<sup>3</sup> This explains the slight differences in impedance computation between otherwise identical regions A and G.

Table 1: Overall Transverse Impedance Coefficients for Different Optics Settings

summary $\beta^* / \text{m}$	$\zeta / (\text{M}\Omega\sqrt{\text{MHz}}/\text{m})$	
	x plane	y plane
0.15	31.58	33.05
0.20	25.02	25.25
<b>0.30</b>	18.47	18.42
1.10	8.03	8.18
<b>4.60</b>	4.66	4.80
6.00	4.56	4.65

Table 2: Summary of results for collision optics in comparison to effective cold beamscreen coefficients at 50 TeV which have been extracted near 1 MHz from the respective spectra [5].

summary insertion	$\zeta / (\text{M}\Omega\sqrt{\text{MHz}}/\text{m})$		$\alpha / (\Omega/\sqrt{\text{MHz}})$
	x plane	y plane	
A	6.89	6.76	0.97
B	0.71	0.62	1.17
D	1.27	1.25	1.93
F	0.17	0.22	1.22
G	6.89	6.79	0.98
H	0.13	0.14	1.28
J	1.81	1.97	3.29
L	0.61	0.68	1.20
all	18.47	18.42	12.03
cold bs. [5]	23.41	43.25	72.81

For **collision optics**, we investigate the “ultimate” lattice with  $\beta^* = 0.3$  m which has been computed to produce higher impedance coefficients than the “baseline” configuration with  $\beta^* = 1.1$  m. A summary of results is shown in Tab. 2.

The overall transverse impedance of insertions is of similar magnitude as that of the arc segments, invoking considerations for reduction, while the comparison yields a smaller ratio for the longitudinal impedance (Tab. 2). The main transverse contributions originate from high  $\beta$  regions in the main experiment insertions A and G (next section) with minor contributions from the injection and additional experimental insertions B and L (not shown due to space limitations).

For **injection optics**, we investigate the lattice configuration with  $\beta^* = 4.6$  m which has been computed to produce higher impedance coefficients than the configuration with  $\beta^* = 6$  m. A summary of results is shown in Tab. 3.

### Main Experiment Insertion Contributions (A & G)

The main experimental regions include chamber shieldings of superconducting magnets assumed at the temperature 50 K, and updated aperture information for thick shieldings

Table 3: Summary of results for injection optics. The  $\alpha$  coefficients are equal to those in table 2. The cold beamscreen coefficients were extracted from impedance spectra [5] for 3.3 TeV.

summary	$\zeta / (\text{M}\Omega\sqrt{\text{MHz}}/\text{m})$		$\alpha / (\Omega/\sqrt{\text{MHz}})$
	x plane	y plane	
insertion			
A	0.42	0.40	0.97
B	0.23	0.22	1.17
D	1.27	1.25	1.93
F	0.17	0.22	1.22
G	0.44	0.41	0.98
H	0.13	0.13	1.28
J	1.81	1.97	3.29
L	0.20	0.20	1.20
all	4.66	4.80	12.03
cold bs. [5]	17.48	32.15	54.20

in this insertion [12] has been included. (Fig. 2). The contribution of both insertions to longitudinal impedance is on an average level (see Tab. 3).

The transverse impedance of main experiment insertions is dominated by the large values of  $\beta$  belonging to the mini- $\beta$  installation around the collision points. Due to their assumed higher resistivity relative to the cold magnets, the impedance contribution of the drift spaces is significant. Stronger focusing for smaller  $\beta^*$  yields higher impedances; a simplified explanation is given by the scaling law of  $\beta(\Delta s) = \beta^* + \Delta s^2/\beta^* \approx \Delta s^2/\beta^*$  in the collision drift space (see Fig. 2). This is also an explanation for the strong dependency of total transverse impedance dependency on  $\beta^*$  (Tab. 1)

As the transverse contributions scale  $\propto b^{-3}$ , a modest increase of apertures in the drift spaces can significantly reduce the transverse impedance contribution from the main experiments.

## SUMMARY

With the considered assumptions and approximations, the transverse wall impedance of all insertions and the considered operation modes is dominated by contributions from

1. drift spaces in the main experiment insertions A and G in collision mode due to focusing into the collision point and relatively small apertures. An increase of drift space apertures could reduce apertures significantly.
2. extraction insertion D, mainly due to necessary moderately large  $\beta$  values in comparison to standard aperture dimensions (not shown due to space limitations). The relative contribution is small for collision mode but relatively large for injection mode. In this insertion, a moderate increase of aperture dimensions could also reduce the impedance contribution of the extraction.

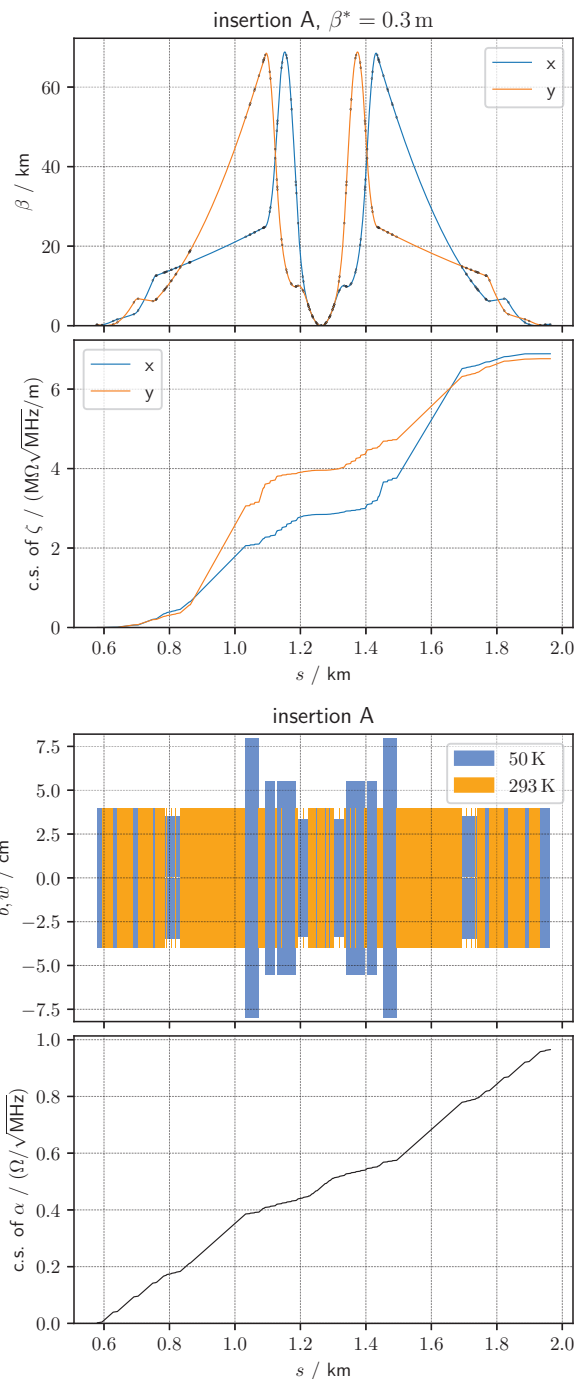


Figure 2:  $\beta$  function [11] and cumulative transverse impedance coefficients (top) respectively temperature assumptions, beam pipe semiaxes, and cumulative longitudinal impedance (bottom) for main experiment insertion A with collision optics.

The complete analysis of the data considered in this work will be published in an upcoming CERN Report.

## ACKNOWLEDGEMENTS

The authors thank A.S. Langner, R. Martin, M. Hofer and O. Boine-Frankenheim for input and helpful discussions.

Work supported by CERN (ref. numbers KE3123, EDMS 1606722) and German Ministry for Education & Research (BMBF, funding code 05P15PERB1).

## REFERENCES

- [1] A. Chance et al., “Updates on the Optics of the Future Hadron-Hadron Collider FCC-hh”, Proc. IPAC17, Copenhagen, Denmark, TUPVA002 (2017) <http://accelconf.web.cern.ch/AccelConf/ipac2017/papers/tupva002.pdf>
- [2] A. Koschik et al., “Transverse Resistive Wall Impedance and Wake Function with Inductive Bypass”, Proc. EPAC 2004, Lucerne, Switzerland, pp. 1876-1878. <http://accelconf.web.cern.ch/AccelConf/e04/PAPERS/WEPLT023.PDF>
- [3] A. Chao, *Physics of Collective Instabilities in Particle Accelerators*, chapter 2 (Wiley, 2003)
- [4] N. Mounet, “The LHC transverse coupled-bunch instability”, PhD thesis (EPFL Lausanne, 2012)
- [5] S. Arsenyev, FCC impedance online database, <https://impedance.web.cern.ch/impedance/fcchh>
- [6] R.L. Gluckstern, J. van Zeijts and B. Zotter, “Coupling impedance of beam pipes of general cross section”, *Phys. Rev. E* **47** (1992) <http://cds.cern.ch/record/238914>
- [7] K. Yokoya, “Resistive wall impedance of beam pipes of general cross section”, *Part. Acc.* **41** (1993), p. 18 – 19. <https://cds.cern.ch/record/248630>
- [8] A. Wolski and D. Newton, “Design of Electron Storage and Damping Rings, part 6”, USPAS 2013, Fort Collins Colorado (2013) <http://uspas.fnal.gov/materials/13CSU/Lecture6.pdf>
- [9] R.A. Matula, “Electrical Resistivity of Copper, Gold, Palladium, and Silver”, Table 2, *J. Phys. Chem. Ref. Data* **8** (4) (1979) <https://srdata.nist.gov/JPCRD/jpcrd155.pdf>
- [10] A.S. Langner, M. Hofer, personal communication (2017)
- [11] A. Chance et al., MAD-X lattice files for FCC-hh commit 5443690ac (2018) <https://gitlab.cern.ch/fcc-optics/FCC-hh-lattice>
- [12] R. Martin, personal communication (2017)